Supporting information

Evolution of Fluoride Shuttle Battery Reaction of BiF_3 Microparticles in a CsF/LiBOB/tetraflyme Electrolyte: Dependence on Structure, Size and Shape

Toshiro Yamanaka,[†*] Asuman Celik Kucuk,[†] Zempachi Ogumi,[†] and Takeshi Abe[‡]

[†]*Office of Society-Academia Collaboration for Innovation, Kyoto University, Katsura, Nishikyo, Kyoto 615-8530, Japan.*

[‡]*Graduate School of Global Environmental Studies, Kyoto University, Katsura, Nishikyo, Kyoto 615-8510, Japan*

[*]e-mail: yamanaka@saci.kyoto-u.ac.jp

1. Raman mapping of (o, c)-BiF_3/gold at OCV

An electrochemical cell with (o.c)-BiF_3/gold was assembled to study the stability of o-BiF_3 and c-BiF_3 in the CsF(sat.)/LiBOB/tetraglyme electrolyte. Raman mapping was conducted while keeping the cell at OCV for more than 9 days. Figures S1a and S1b show results within one hour and at nine days after assembling the cell. No significant change was observed. Non-electrochemical transformation from o-BiF_3 to c-BiF_3 that was previously observed in the ionic liquid electrolyte did not occur.

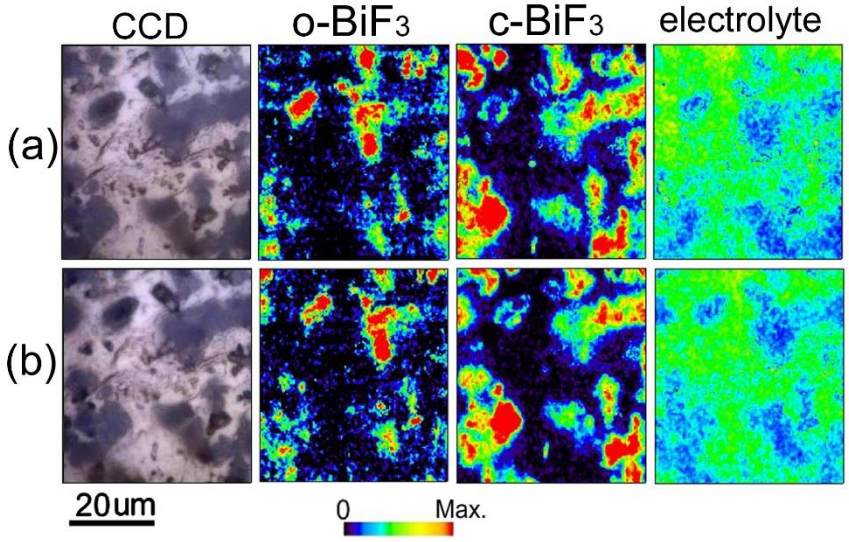

Figure S1. Results of Raman mapping while keeping (o, c)-BiF_3/gold at OCV in the CsF(sat.)/LiBOB/tetraglyme electrolyte. Results obtained within one hour (a) and at 9 days after assembling the cell.

2. Voltage and current during Raman mapping of a large o-BiF_3 particle on o-BiF_3/gold during defluorination.

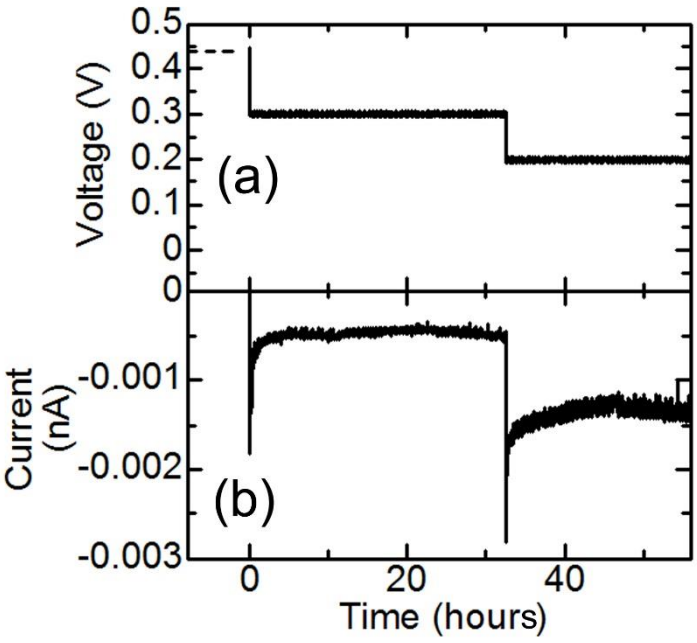

Figure S2. Voltage applied and current during Raman mapping of o-BiF_3/gold shown in Fig. 5 in the main text.

3. Voltage and current during Raman mapping of a large c-BiF_3 particle on c-BiF_3/gold during defluorination.

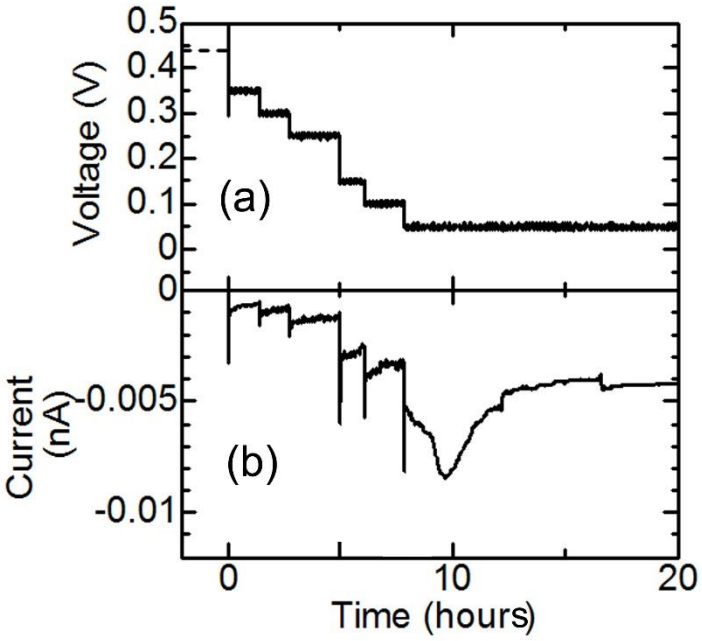

Figure S3. Voltage applied and current during Raman mapping of c-BiF_3/gold shown in Fig. 6 in the main text.

4. Voltage and current during Raman mapping of small o-BiF_3 particles on o-BiF_3/gold during defluorination.

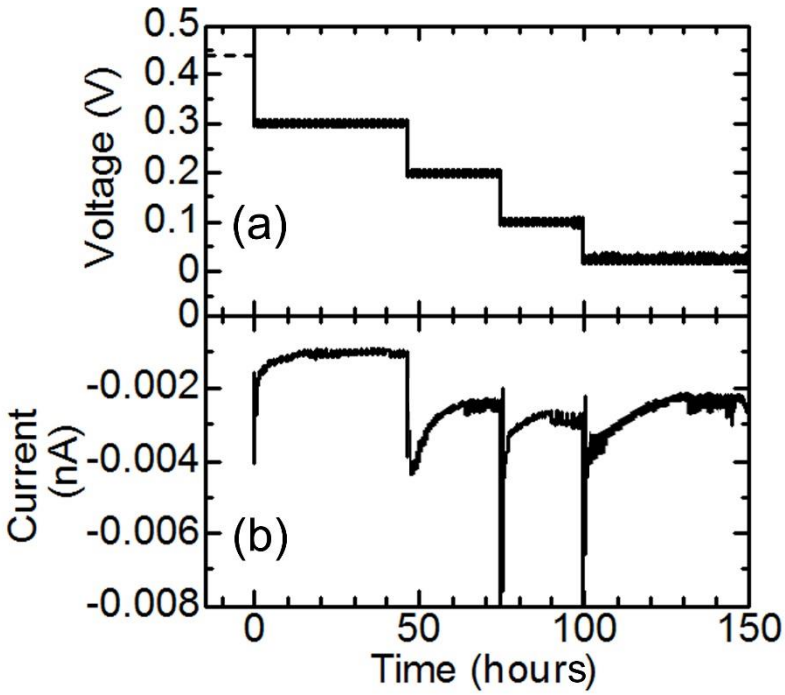

Figure S4. Voltage applied and current during Raman mapping of o-BiF_3/gold shown in Fig. 7 in the main text.

5. Raman mapping during fluorination of Bi on c-BiF_3/gold after defluorination

In situ Raman mapping during fluorination of Bi was conducted using the same c-BiF_3/gold sample after defluorination as that shown in Fig. 4c and 4d in the main text.

Figure S5a and S5b show voltage applied to the cell and resultant current, respectively. Figure. S5c shows a CCD image, mappings for c-BiF_3 and Bi, and superposition of the CCD image and the mapping for Bi, which were taken within one hour from the voltage change to 0.65 V. Figure. S5d shows results after 48 hours from the voltage change to 0.65 V. Decrease in areas of the peak for c-BiF_3 and increase in areas of the peak for Bi were observed, as indicated by white arrows. In many cases with various electrolytes, fluorination of Bi was not clearly observed by Raman spectroscopy. Since the area of c-BiF_3 increased only at the positions of particles, not on the gold substrate, it is concluded that fluorination proceeded by the direct mechanism (reverse of eq. (1) in the main text).

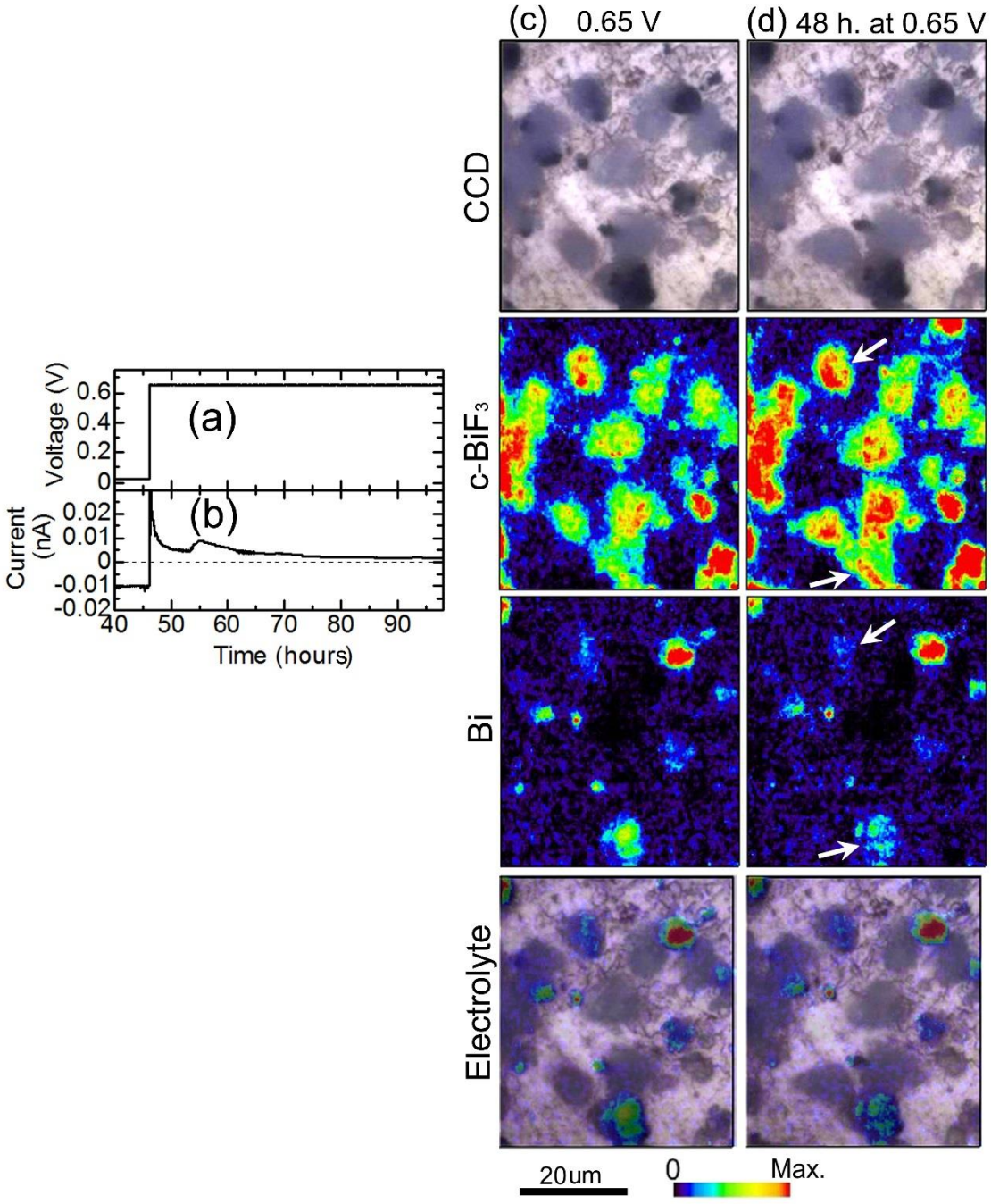

Figure S5. Voltage to induce fluorination applied to c-BiF_3/gold (a) and the resultant current (b) after defluorination shown in Fig. 4 in the main text. CCD image, mappings for c-BiF_3 and Bi, and superposition of the CCD image and the mapping for Bi taken within one hour (c) and after 48 hours (d) from the voltage change to 0.65 V.

6. Raman mapping during defluorination of o-BiF_3 and c-BiF_3 on (o,c)-BiF_3/gold in CsF(0.5 sat.)/LiBOB/G4

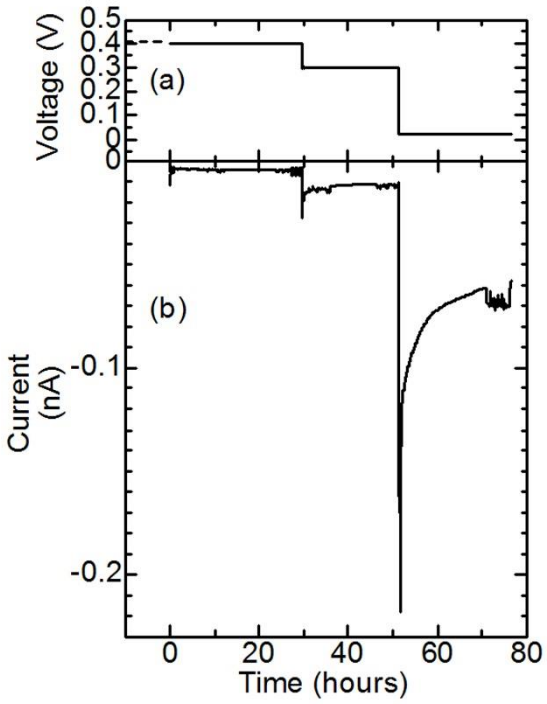

Figure S6. (a) shows the voltage applied to induce defluorination of o-BiF_3 and c-BiF_3 on (o,c)-BiF_3/gold in CsF(0.5 sat.)/LiBOB/G4. (b) shows the current due to defluorination.

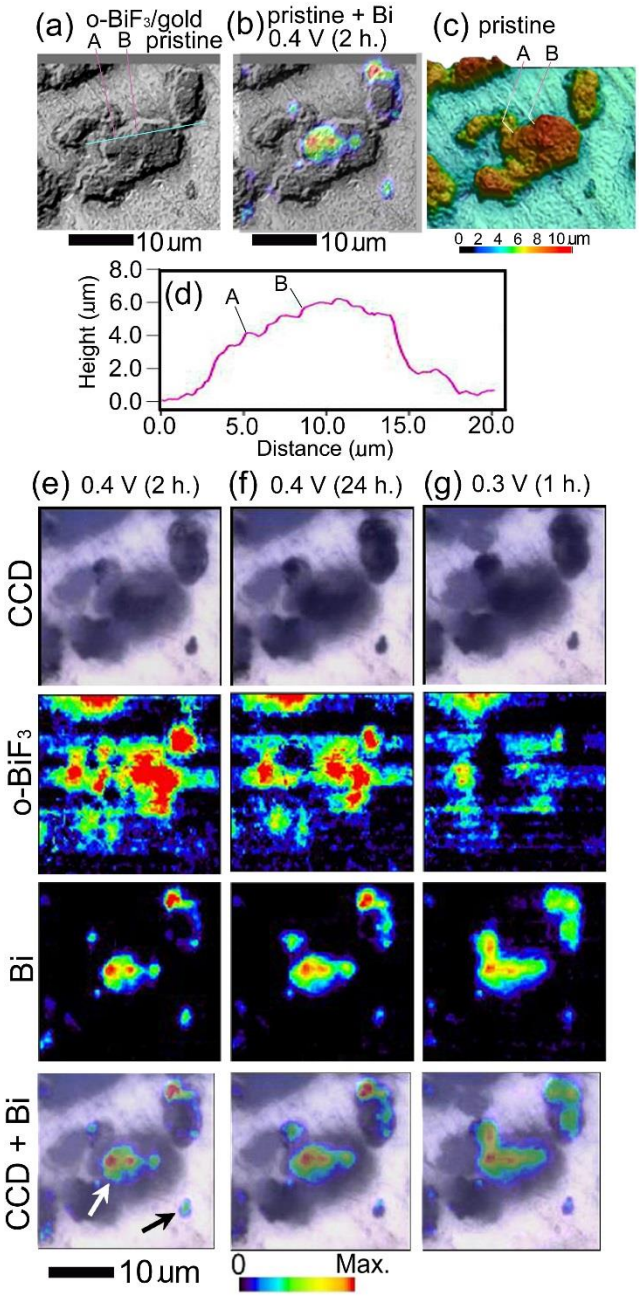

Figure S7. Relation between evolution of defluorination and morphology of a large o-BiF_3 particle in CsF(0.5 sat.)/LiBOB/G4. LSCM images (a,b) and a 3D-bird's eye view (c) of a large o-BiF_3 particle on the surface of an (o,c)-BiF_3/gold sample, taken in air before construction of a cell. There are protrusions at the top of the particle that are far from the contours of the particle (gold current collector) as indicated by A and B in (a) and (c). (d) shows a height profile along the blue line in (a). (e)-(g) show results at the voltages indicated. CCD images, mappings of areas of peaks for o-BiF_3 and Bi, and superposition of the CCD images and the mappings for Bi are shown. In (e), defluorination at the protrusions far from the contours is seen (white arrow) and is superposed on the LSCM image in (b). Defluorination of the small particle proceeded fast (black arrow). Bi was not detected on the gold plating, indicating the direct defluorination mechanism.

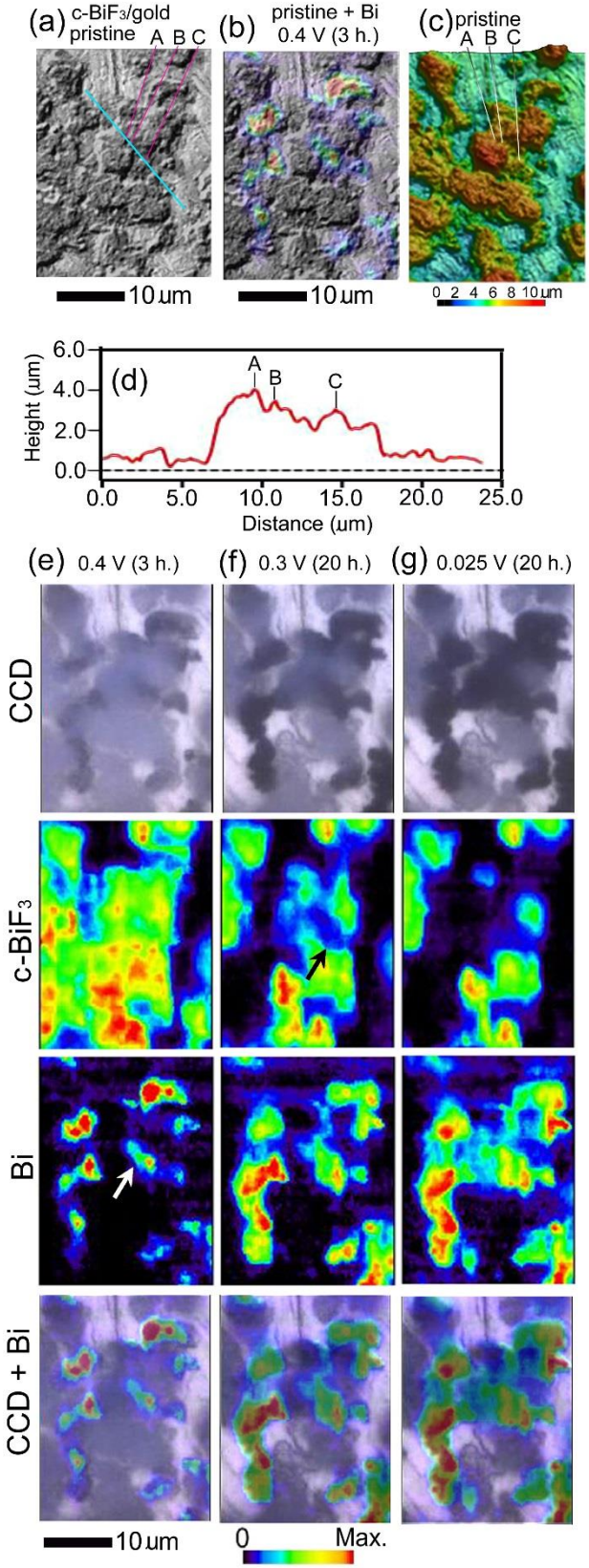

Figure S8. Relation between evolution of defluorination and morphology of a large c-BiF_3 particle in CsF(0.5 sat.)/LiBOB/G4. LSCM images (a,b) and a 3D-bird's eye view (c) of a large c-BiF_3 particle on the surface of an (o,c)-BiF_3/gold sample, taken in air before construction of a cell. There are protrusions at the top of the particle that are far from the contours of the particle (gold current collector) as indicated by A, B and C in (a)

and (c). (d) shows a height profile along the blue line in (a). (e)-(g) show results at the voltages indicated. CCD images, mappings of areas of peaks for c-BiF_3 and Bi, and superposition of the CCD images and the mappings for Bi are shown. In (e), defluorination at the protrusions far from the contours is seen (white arrow) and is superposed on the LSCM image in (b). The black arrow in (f) indicates a hole-like decrease of the area of the peak for c-BiF_3 at the protrusions A, B and C.

7. Raman mapping during defluorination of o-BiF_3 and c-BiF_3 on (o,c)-BiF_3/gold in CsF (0.25 sat.)/LiBOB/G4

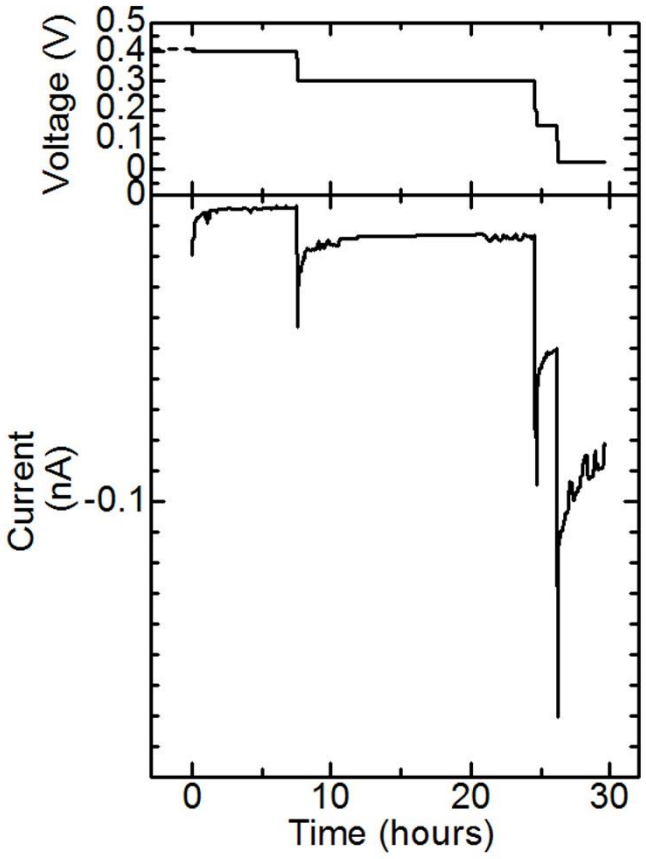

Figure S9. (a) shows the voltage applied to induce defluorination of o-BiF_3 and c-BiF_3 on (o,c)-BiF_3/gold in CsF(0.25 sat.)/LiBOB/G4. (b) shows the current due to defluorination.

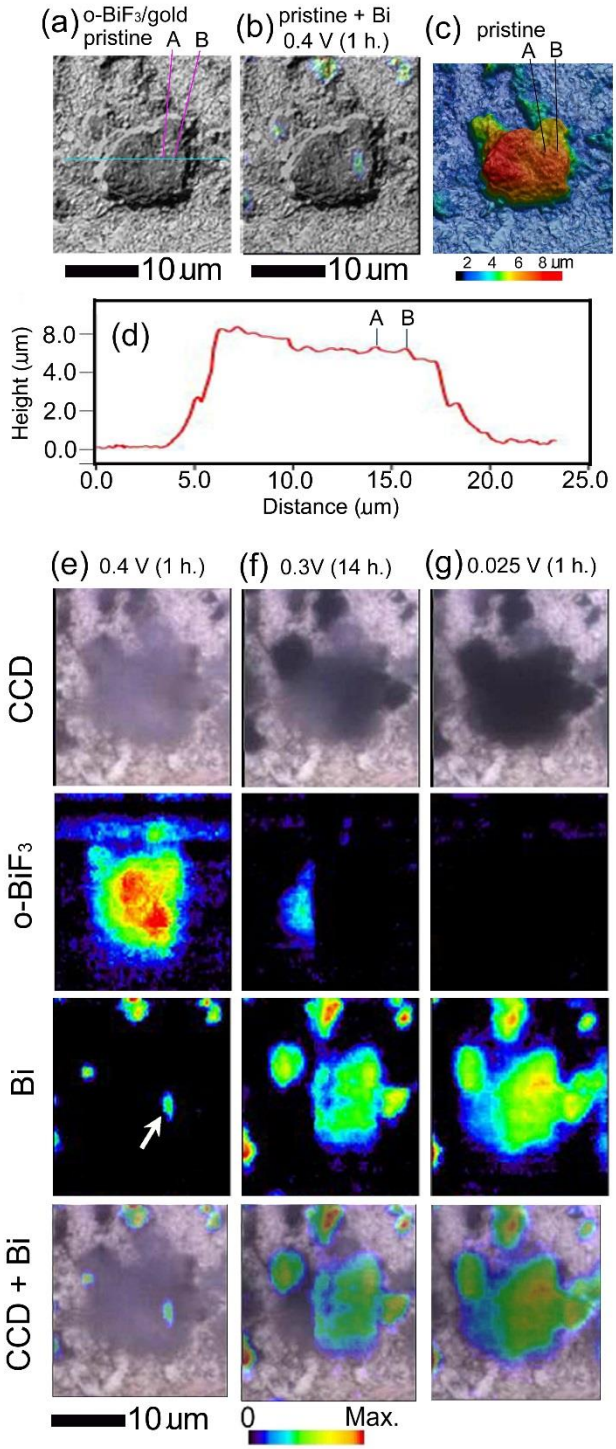

Figure S10. Relation between evolution of defluorination and morphology of a large o-BiF_3 particle in CsF(0.25 sat.)/LiBOB/G4. LSCM images (a,b) and a 3D-bird's eye view (c) of a large o-BiF_3 particle on the surface of an (o,c)-BiF_3/gold sample, taken in air before construction of a cell. There are protrusions at the top of the particle as indicated by A and B in (a) and (c). (d) shows a height profile along the blue line in (a). (e)-(g) show results at the voltages indicated. CCD images, mappings of areas of peaks for o-BiF_3 and Bi, and superposition of the CCD images and the mappings for Bi are shown. In (e),

defluorination at the protrusions far from the contours is seen (white arrow) and is superposed on the LSCM image in (b). Bi was not detected on the gold plating, indicating the direct defluorination mechanism.

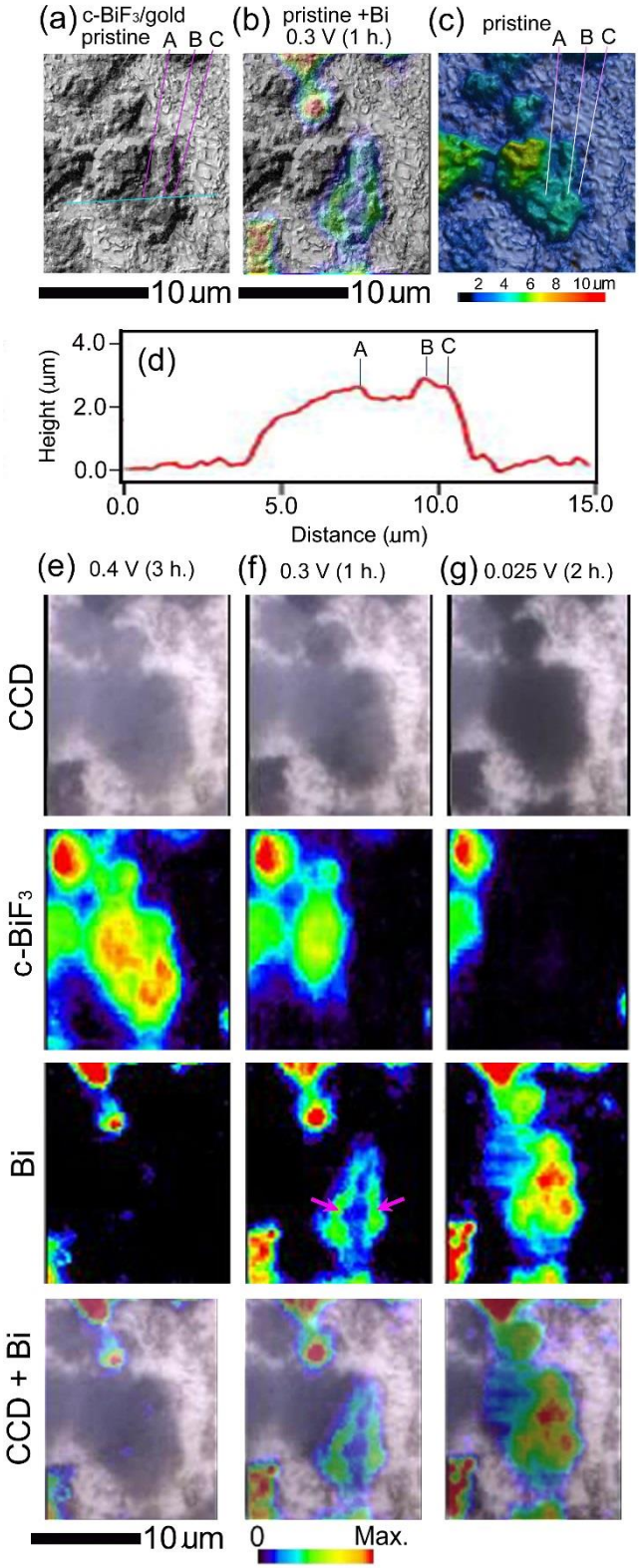

Figure S11. Relation between evolution of defluorination and morphology of a large c-BiF_3 particle in CsF(0.25 sat.)/LiBOB/G4. LSCM images (a,b) and a 3D-bird's eye view (c) of a large c-BiF_3 particle on the surface of an (o,c)-BiF_3/gold sample, taken in air before construction of a cell. There are protrusions at the top of the particle as indicated by A, B and C in (a) and (c). (d) shows a height profile along the blue line in (a). (e)-(g) show results at the voltages indicated. CCD images, mappings of areas of peaks for o-BiF_3 and Bi, and superposition of the CCD images and the mappings for Bi are shown. In (f), defluorination at the protrusions is seen (red violet arrows) and is superposed on the LSCM image in (b).

8. Raman mapping during defluorination of o-BiF_3 and c-BiF_3 on (o,c)-BiF_3/gold in LiBOB/G4 without CsF

A cell was constructed using (o,c)-BiF_3/gold and LiBOB(0.25 M)/G4 without CsF, and the value of OCV was about 0.41 V. Defluorination of o-BiF_3 and c-BiF_3 was observed as the voltage was decreased. Thus, Raman mapping was conducted during this process to study the mechanism of defluorination.

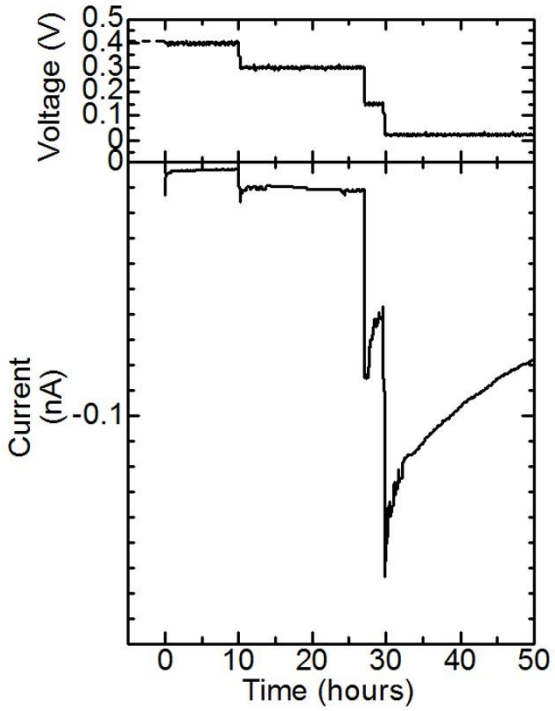

Figure S12. (a) shows the voltage applied to induce defluorination of o-BiF_3 and c-BiF_3 on (o,c)-BiF_3/gold in LiBOB/G4. (b) shows the current due to defluorination.

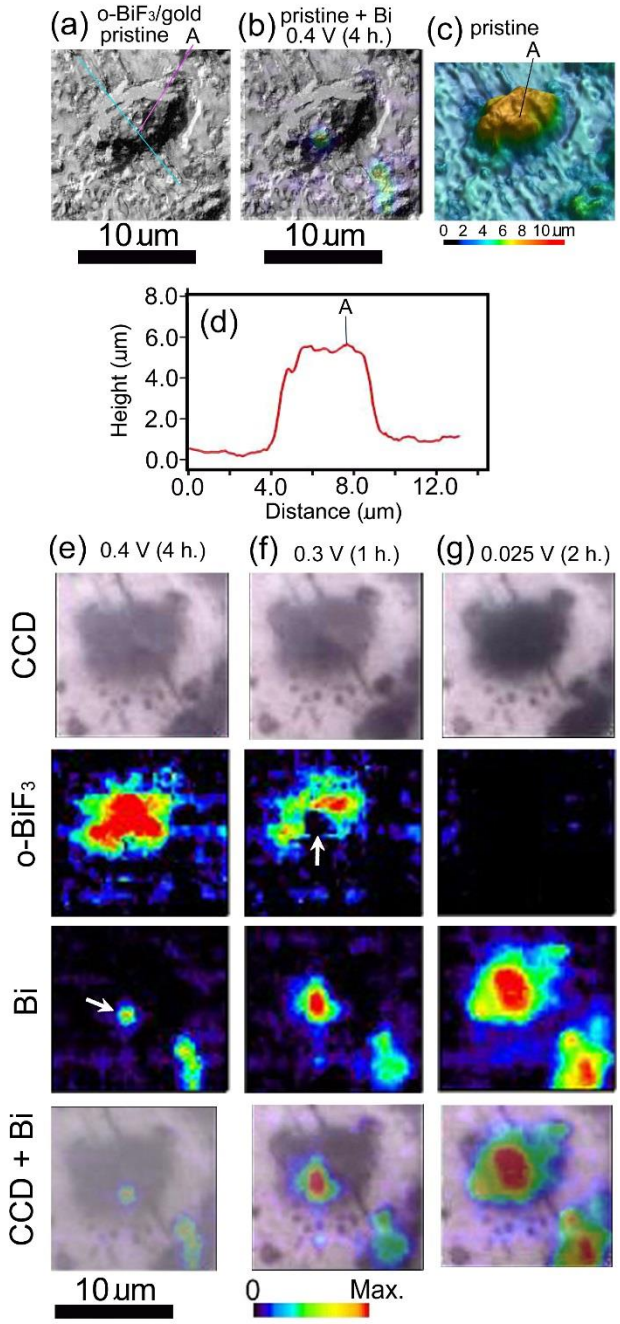

Figure S13. Relation between evolution of defluorination and morphology of a large o-BiF_3 particle in LiBOB/G4. LSCM images (a,b) and a 3D-bird's eye view (c) of a large o-BiF_3 particle on the surface of an (o,c)-BiF_3/gold sample, taken in air before construction of a cell. There is a protrusion at the top of the particle as indicated by A in (a) and (c). (d) shows a height profile along the blue line in (a). (e)-(g) show results at the

voltages indicated. CCD images, mappings of areas of peaks for o-BiF_3 and Bi, and superposition of the CCD images and the mappings for Bi are shown. In (e), defluorination at the protrusion far from the contours is seen (white arrow) and is superposed on the LSCM image in (b). In (f), there is a hole-like decrease in the area of the peak for o-BiF_3 due to defluorination (white arrow). Bi was not detected on the gold plating, indicating the direct defluorination mechanism.

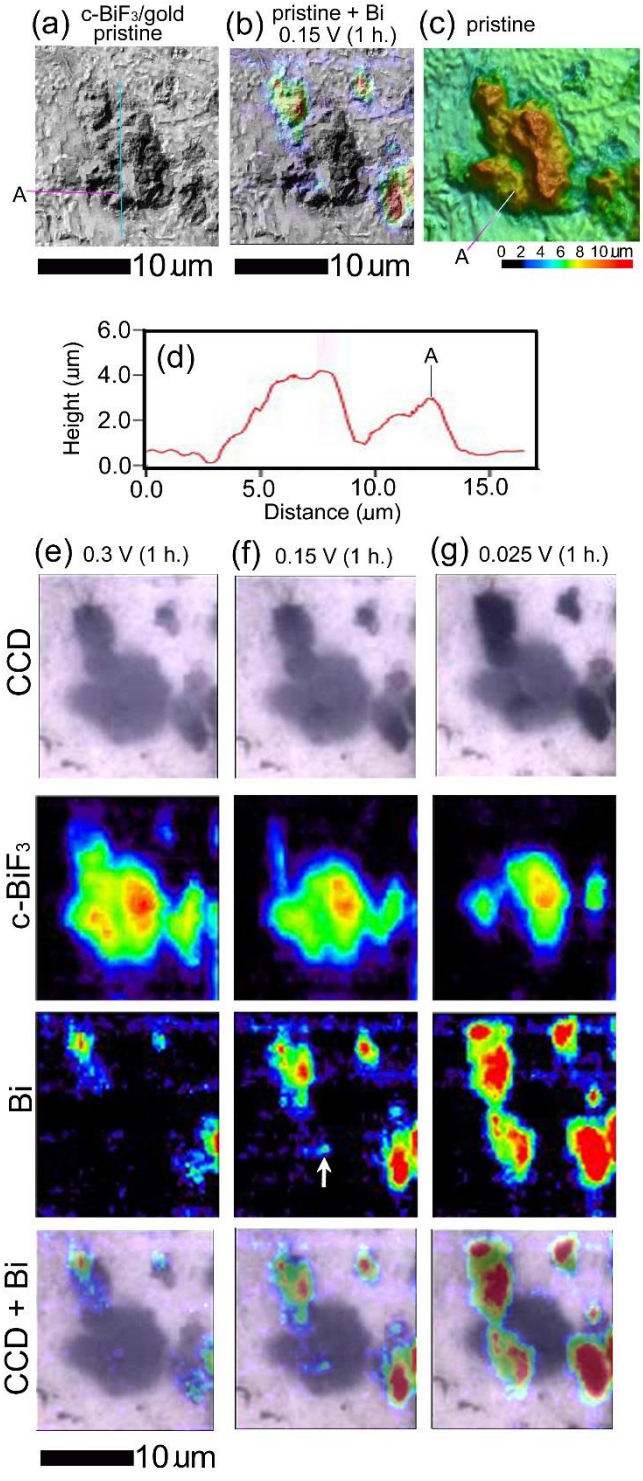

Figure S14. Relation between evolution of defluorination and morphology of a large c-BiF_3 particle in LiBOB/G4. LSCM images (a,b) and a 3D-bird's eye view (c) of a large c-BiF_3 particle on the surface of an (o,c)-BiF_3/gold sample, taken in air before construction of a cell. There is a protrusion at the top of the particle as indicated by A in (a) and (c). (d) shows a height profile along the blue line in (a). (e)-(g) show results at the voltages indicated. CCD images, mappings of areas of peaks for c-BiF_3 and Bi, and superposition of the CCD images and the mappings for Bi are shown. In (f), defluorination at the protrusion far from the contours is seen (white arrow) and is superposed on the LSCM image in (b).

9. Solubilities of Bi and BiF_3 in CsF/LiBOB/G4 with various concentrations of CsF

Solubilities of Bi and BiF_3 were determined by atomic absorption spectroscopy (AAS) with Za3000 (Hitachi High-Technologies). BiF_3 or Bi was immersed in CsF(sat.)/LiBOB/G4, CsF(0.5 sat.)/LiBOB/G4, CsF(0.25 sat.)/LiBOB/G4, CsF(0.125 sat.)/LiBOB/G4 and LiBOB/G4 (See the experimental section in the main text.) for one week, and concentrations of Bi in their supernatants were analyzed by AAS. The concentration of Cs in CsF(sat.)/LiBOB/G4 was previously determined by AAS to be 4.4×10^{-3} M.[17] The results showed that the solubilities of BiF_3 and Bi in these electrolytes are always below 4.78×10^{-6} M (This corresponds to 1 ppm of Bi.).

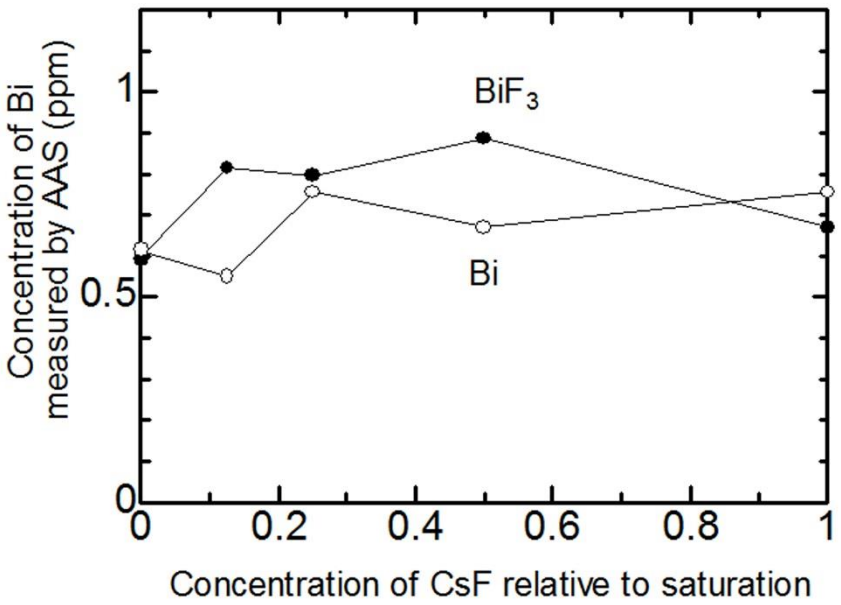

Figure S15. Concentrations of Bi in CsF(sat.)/LiBOB/G4, CsF(0.5 sat.)/LiBOB/G4, CsF(0.25 sat.)/LiBOB/G4, CsF(0.125 sat.)/LiBOB/G4 and LiBOB/G4 electrolytes after

immersing BiF_3 or Bi in these electrolytes for one week measured by AAS. Concentration of CsF at saturation was reported to be 4.4×10^{-3} M.[17]

10. DFT calculation of energies and densities of states of o-BiF_3 and c-BiF_3

Energies and densities of states of o-BiF_3 and c-BiF_3 were calculated by Materials Studio CASTEP code, which is a first-principles density functional theory (DFT) method. The on the fly generated (OTFG) norm-conserving pseudopotential was used for electron−ionic core interactions. Generalized gradient approximation (GGA)-PBE was used to approximate exchange and correlation energies. A method proposed by Koelling and Harmon was used to take into account the effect of theory of relativity for states of valence electrons. The total energies due to electrons were calculated to be **-10591.10099103 eV for o-BiF_3 and -10587.04716497 eV for c-BiF_3 per unit cell** (containing 4 Bi and 12 F atoms)**.** The energy of o-BiF_3 is lower than that of c-BiF_3 by about 4 V, leading to a potential for defluorination of o-BiF_3 lower than that of c-BiF_3 by about 0.33 V, which is opposite to the experimental results.

Free energies due to phonons of o-BiF_3 and c-BiF_3 were also calculated. Results are shown in Fig. S16. The free energy due to phonons of o-BiF_3 is lower than that of c-BiF_3 by about 0.15 V per unit cell at 300 K. These results cannot explain the faster defluorination rate of o-BiF_3 than that of c-BiF_3.

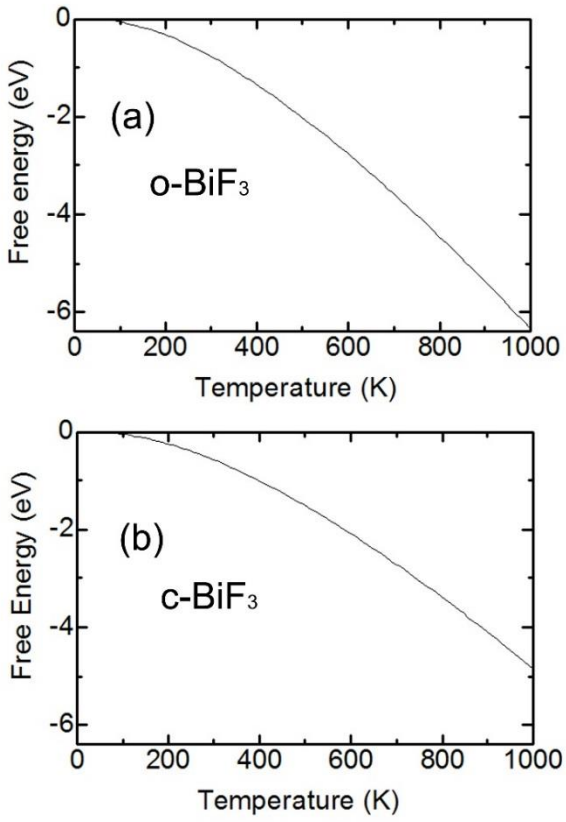

Figure S16. Free energies due to phonons of o-BiF_3 and c-BiF_3 against temperature.

Densities of states of electrons of o-BiF_3 and c-BiF_3 were calculated. Results are shown in Fig. S17. The values for band gaps of o-BiF_3 and c-BiF_3 are about 4.4 V and 3.8 V, respectively, suggesting lower electron conductivity of o-BiF_3, which cannot explain the faster defluorination rate of o-BiF_3 than that of c-BiF_3.

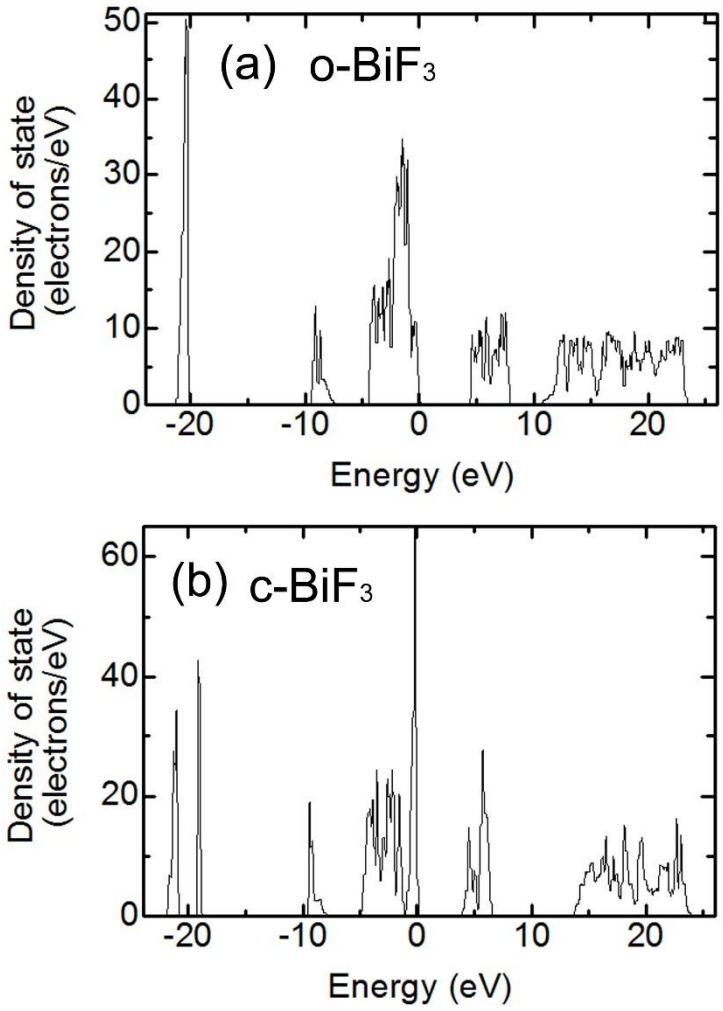

Figure S17. Densities of states of electrons of (a) o-BiF_3 and (b) c-BiF_3.